Earth Planets Space, **55**, 395–404, 2003

A representation function for a distribution of points on the unit sphere—with applications to analyses of the distribution of virtual geomagnetic poles

Ji-Cheng Shao[1], Yozo Hamano[1], Michael Bevis[2], and Michael Fuller[2]

[1]*Department of the Earth and Planetary Science, University of Tokyo, Japan*
[2]*HIGP/SOEST, University of Hawaii, USA*

(Received November 15, 2002; Revised July 14, 2003; Accepted July 22, 2003)

An arbitrary point distribution consisting of a finite number of points on a unit sphere may be completely and uniquely represented by an analytic function in the form of a spherical harmonic expansion. The applications of this representation function are illustrated in an analysis of the symmetries in the virtual geomagnetic pole (VGP) distribution of the polarity reversal records of the past 10 million years. We find that the longitudinal confinements in the VGP distribution are (a) persistent only in the equatorially symmetric part (of the non-zonal symmetries) of the VGP distribution and (b) strong along the east coast of the North American continent and weak along the longitudes of East Asia-Australia. We also find that the equatorially symmetric patterns in the VGP distribution appear to extend preferentially into the Pacific Ocean and are relatively depleted in the longitude band associated with Africa.

Key words: Virtual geomagnetic pole, geomagnetic reversal, representation function.

1. Introduction

The problem of analyzing the spatial distribution of a set of points on the unit sphere arises in many fields of physical and natural science (Fisher *et al.*, 1987). Frequently the points represent the orientation of vectors (e.g. arrival directions) or of undirected lines (e.g. stress axes). In other cases the points represent the positions of objects or events (e.g. VGPs and earthquake epicenters). While spherical data sets of this kind can be analyzed as point distributions *per se*, more typically the analyst assumes that the point set reflects or samples a population or a statistical distribution characterized by a continuous probability density function (PDF). In some cases, it is possible to model the point set using a standard statistical distribution, such as the Fisher, Watson or Bingham distribution (Fisher *et al.*, 1987). These distributions have few parameters and fairly simple (often highly symmetric) density functions. In cases where the density of points varies in an irregular or complex fashion, and cannot be represented using standard spherical distributions, analysts may construct a non-parametric PDF by using numerical procedures. In this paper we introduce an alternative analytical function that can completely and uniquely represent a point set with arbitrarily complex spatial structure on the unit sphere. We then demonstrate this function by applying it to depict various symmetries in the VGP distribution and to evaluate biases in the VGP distribution of the polarity reversals of the Earth's magnetic field for the past 10 million years.

2. The Representation Function for a Point Distribution on the Unit Sphere

Our starting point is the Dirac delta function for a point $\hat{\mathbf{p}}_0$ on the unit sphere,

$$\delta(\hat{\mathbf{p}}_0, \hat{\mathbf{r}}) = \frac{1}{4\pi} \sum_{l=0}^{\infty} \sum_{m=-l}^{l} \overline{Y_l^m(\hat{\mathbf{p}}_0)} Y_l^m(\hat{\mathbf{r}}), \tag{1}$$

where $Y_l^m(\hat{\mathbf{r}})$ is the fully normalized surface spherical harmonic of degree l and order m, and $\overline{Y_l^m(\hat{\mathbf{r}})}$ is the complex conjugate of $Y_l^m(\hat{\mathbf{r}})$. The Dirac delta function satisfies $\delta(\hat{\mathbf{p}}_0, \hat{\mathbf{r}}) = \infty$, if $\hat{\mathbf{r}} = \hat{\mathbf{p}}_0$, and $\delta(\hat{\mathbf{p}}_0, \hat{\mathbf{r}}) = 0$, if $\hat{\mathbf{r}} \neq \hat{\mathbf{p}}_0$. Next we define a function $T^{(L)}(\hat{\mathbf{r}})$,

$$T^{(L)}(\hat{\mathbf{r}}) = \frac{1}{(L+1)^2} \sum_{l=0}^{L} \sum_{m=-l}^{l} \overline{Y_l^m(\hat{\mathbf{p}}_0)} Y_l^m(\hat{\mathbf{r}}). \tag{2}$$

Using the identity,

$$\sum_{l=0}^{L} \sum_{m=-l}^{l} \left| Y_l^m(\hat{\mathbf{p}}_0) \right|^2 = \sum_{l=0}^{L} (2l+1) = (L+1)^2,$$

We obtain $T^{(L)}(\hat{\mathbf{p}}_0) = 1$. We then define the function

$$T(\hat{\mathbf{r}}) = \lim_{L \to \infty} T^{(L)}(\hat{\mathbf{r}}). \tag{3}$$

From (1) and (2), the function $T^{(L)}(\hat{\mathbf{r}})$ satisfies $T(\hat{\mathbf{p}}_0) = 1$, and $T(\hat{\mathbf{r}}) = 0$ for every $\hat{\mathbf{r}} \neq \hat{\mathbf{p}}_0$. $T(\hat{\mathbf{r}})$ represents the distribution of a single point on the unit sphere. We now generalize this analysis so as to consider a finite set of points on the unit sphere. Let $P = [\hat{\mathbf{p}}_1, \hat{\mathbf{p}}_2, \ldots, \hat{\mathbf{p}}_i, \ldots, \hat{\mathbf{p}}_K]$ be a set of K distinct points on the unit sphere. We allow for coincident or duplicate points by introducing a set of point counts $N = [n_1, n_2, \ldots, n_i, \ldots, n_K]$, where n_i represents

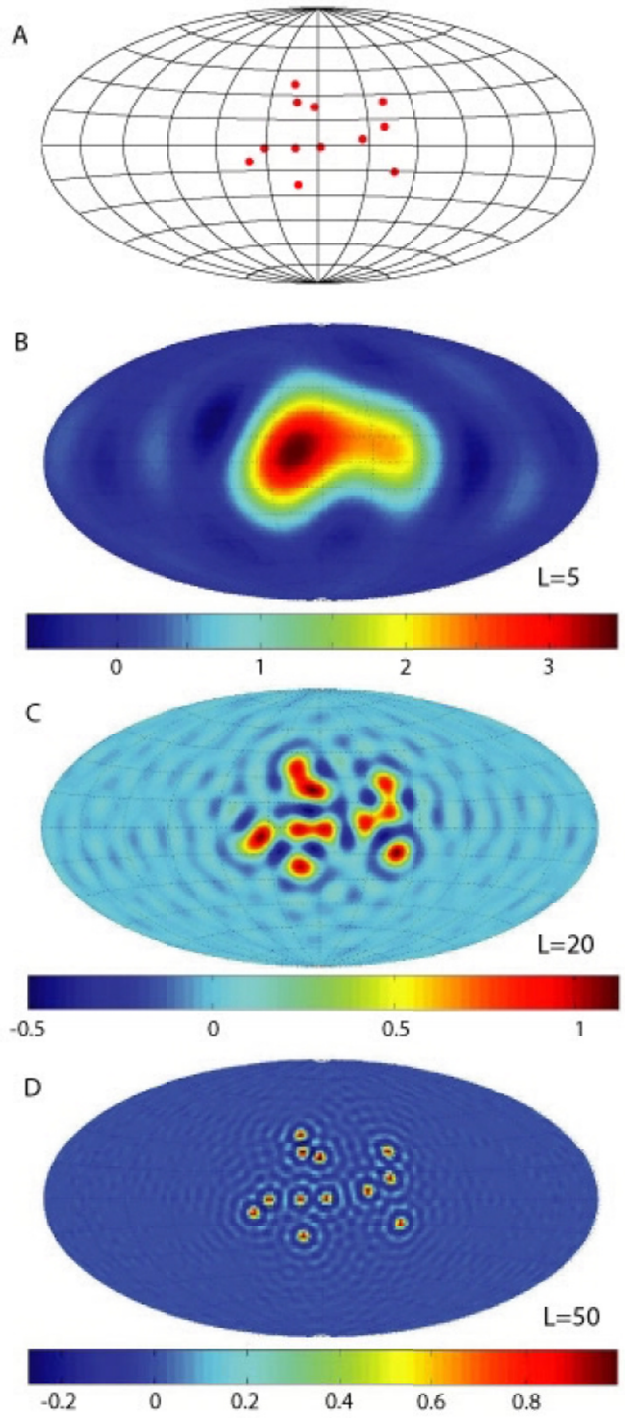

Fig. 1. A set of 12 points are located at centers of the red circles in (a). Truncated representation functions for this point set are shown in (b)–(d). They are (b) $D^{(5)}(\hat{\mathbf{r}})$, (c) $D^{(20)}(\hat{\mathbf{r}})$, and (d) $D^{(50)}(\hat{\mathbf{r}})$. (The colours in all maps given in this paper are linearly scaled.)

the number of points at $\hat{\mathbf{p}}_i$, $n_i \geq 1$ for any $n_i \in N$, and the total number of points is

$$n = \sum_{i=1}^{K} n_i .$$

We construct a distribution function for the point set $P : N$ by combining the distribution functions for the individual points defined in (2). We define

$$D^{(L)}(\hat{\mathbf{r}}) = \sum_{i=1}^{K} n_i T_i^{(L)}(\hat{\mathbf{r}}).$$

Substituting for $T^{(L)}(\hat{\mathbf{r}})$ using (2), and defining the coefficients,

$$d_l^m = \sum_{i=1}^{K} n_i \overline{Y_l^m(\hat{\mathbf{p}}_i)}, \tag{4}$$

$D^{(L)}(\hat{\mathbf{r}})$ can be expressed as,

$$D^{(L)}(\hat{\mathbf{r}}) = \frac{1}{(L+1)^2} \sum_{l=0}^{L} \sum_{m=-l}^{l} d_l^m Y_l^m(\hat{\mathbf{r}}). \tag{5}$$

Finally we can write the representation function for the point distribution $P : N$ as

$$D(\hat{\mathbf{r}}) = \lim_{L\to\infty} D^{(L)}(\hat{\mathbf{r}}). \tag{6}$$

Function $D(\hat{\mathbf{r}})$ satisfies $D(\hat{\mathbf{p}}_i) = n_i$ for every $\hat{\mathbf{p}}_i \in P$, and $D(\hat{\mathbf{r}}) = 0$ elsewhere on the unit sphere. Hence $D(\hat{\mathbf{r}})$ completely represents the point distribution. The uniqueness of $D(\hat{\mathbf{r}})$ is obvious from Eq. (4) since for a given point set there is one and only one set of coefficients d_l^m. Each of the coefficients d_l^m is determined independent of the determination of the other coefficients. Every coefficient d_l^m is exact, if the positions of the points are given exactly. If the positions of the points contain errors, then a mean and a variance may be associated with every d_l^m. But there is no covariance associated with d_l^m (because each d_l^m is determined independently). In this paper, we always assume that the positions of the points are exact.

In practice, we can only use $D^{(L)}\left(\hat{\mathbf{r}}\right)$ instead of $D(\hat{\mathbf{r}})$ to represent the point distribution. $D^{(L)}\left(\hat{\mathbf{r}}\right)$ is an image of the point distribution. The spatial resolution of $D^{(L)}\left(\hat{\mathbf{r}}\right)$ is given by $180^\circ/(L+0.5)$ which is the minimum half spatial wavelength in the spherical harmonic expansion up to degree L (Backus *et al.*, 1996). $D^{(L)}\left(\hat{\mathbf{r}}\right)$ is, in a sense, "a blurred view (of the point distribution) obtained by a myopic observer who has forgotten his or her glasses" (Backus *et al.*, 1996). The selection of a proper truncation level L is always subjective, and there is not an ideal or even optimal L which may be selected in a purely objective context (perhaps, except $L = \infty$). One of the useful parameters for selecting a proper L is the power spectrum of d_l^m defined by,

$$p_l = \sum_{m=-l}^{l} \left(d_l^m\right)^2. \tag{7}$$

p_l is proportional to the contributions from the symmetries of degree l to the point distribution. L should be chosen such that $D^{(L)}\left(\hat{\mathbf{r}}\right)$ includes the primary symmetries with large p_l. But in some cases, the analyses may require that the point distribution be approximated at different truncation levels.

Because of the finite spherical harmonic truncation, every point in the point distribution is represented by a "wavelet" $T^{(L)}(\hat{\mathbf{r}})$ in (2) to approximate a unit "spike" $T(\hat{\mathbf{r}})$ in (3). This "wavelet" is symmetrical about that point and is unit at the point. The propagations of $T^{(L)}(\hat{\mathbf{r}})$ away from the point are isotropic and oscillatory in all directions with decaying magnitudes. Since $D^{(L)}(\hat{\mathbf{r}})$ is a sum of all $T^{(L)}(\hat{\mathbf{r}})$ on the unit sphere, it is also oscillatory. The larger positive magnitudes in $D^{(L)}(\hat{\mathbf{r}})$ (often significantly larger than the others while a reasonable L is chosen) are associated with the areas where the points are relatively densely populated. The magnitudes of the secondary and the high order signals in $D^{(L)}(\hat{\mathbf{r}})$ are often small, and can be made as small as one pleases by increasing L. They are usually associated with the areas where the points are relatively less populated and where no point is distributed. The secondary and the higher order signals can be either positive or negative, corresponding to the relative magnitudes of the accretions and the depletions of the points respectively. If one wishes to analyze only the accretions of the points in the map of $D^{(L)}(\hat{\mathbf{r}})$, one can then justify to substitute $D^{(L)}(\hat{\mathbf{r}}) = 0$ for the value of $D^{(L)}(\hat{\mathbf{r}})$ which is less than a chosen small positive number or zero (so as to remove all negatives and some of the undesirable small positives). (Note, the negativity in $D^{(L)}\left(\hat{\mathbf{r}}\right)$ is not an unusual situation. For instance, any positive kernel used in geophysics, such as the Dirac delta function $\delta(\hat{\mathbf{p}}_0, \hat{\mathbf{r}})$, may not always be positive everywhere in the numerical computations because of the finite spherical harmonic truncation.)

We illustrate $D^{(L)}\left(\hat{\mathbf{r}}\right)$ by using an artificial example consisting of 12 points on the unit sphere as shown in Fig. 1(a). This point distribution is progressively approximated by $D^{(L)}\left(\hat{\mathbf{r}}\right)$ with $L = 5$, 20, 50 shown in Fig. 1(b), 1(c) and 1(d) respectively. $D^{(50)}\left(\hat{\mathbf{r}}\right)$ has near zero values except at the locations near the points where it rises to nearly unit value, and is recognizably a fuzzy and approximate representation of $D(\hat{\mathbf{r}})$. All point distributions discussed in this paper are geometrical objects. Their representation functions have no units. The colors associated with each figures are linearly scaled between the maximum and the minimum values of the representation functions respectively. The scales in Fig. 1(b), 1(c) and 1(d) may be roughly (empirically) read as the spatial distribution of the number of points in Fig. 1(a) seen in the images with spatial resolutions defined by L. For instance, when the point distribution in Fig. 1(a) is observed under the spatial resolution defined by $L = 15$, the average number of points found in the area defined by the red patch in Fig. 1(b) is roughly 3. As the spatial resolution increasing to $L = 20$ (this roughly means that "window size/bandwidth" decreases), average number of points found in the areas defined by the red patches in Fig. 1(c) is roughly little over 1. As the spatial resolution continuously increasing to infinity (as "window size/bandwidth" decreasing to zero), the number of point found at any location equals to the number of points being distributed there—that is the representation function replicates the point distribution (in Fig. 1(a)).

One of the applications of the representation function in (6) is to separate various symmetries in a point distribution. According to (6), any point distribution on the unit sphere consists of an infinite series of geometrical symmetries defined by an infinite series of $\{d_l^m\, Y_l^m(\hat{\mathbf{r}})\}$. These symmetries are the intrinsic geometrical properties of the point distribution in a given spherical coordinate system. They are often categorized in to various subgroups. Each of the subgroups consists of the symmetries that share some common geometrical properties. For instance, the symmetries of any point distribution on the unit sphere can be completely characterized by two subgroups: the zonal symmetries—all terms in (6) satisfying $m = 0$, and the non-zonal symmetries—all terms in (6) satisfying $m \neq 0$. The subgroup of the zonal symmetries describes the properties of a point distribution that are only latitudinally dependent. The subgroup of the non-zonal symmetries describes the properties of a point distribution that are both latitudinally and longitudinally dependent. We utilize these subgroups to understand the complex geometrical properties of the point distribu-

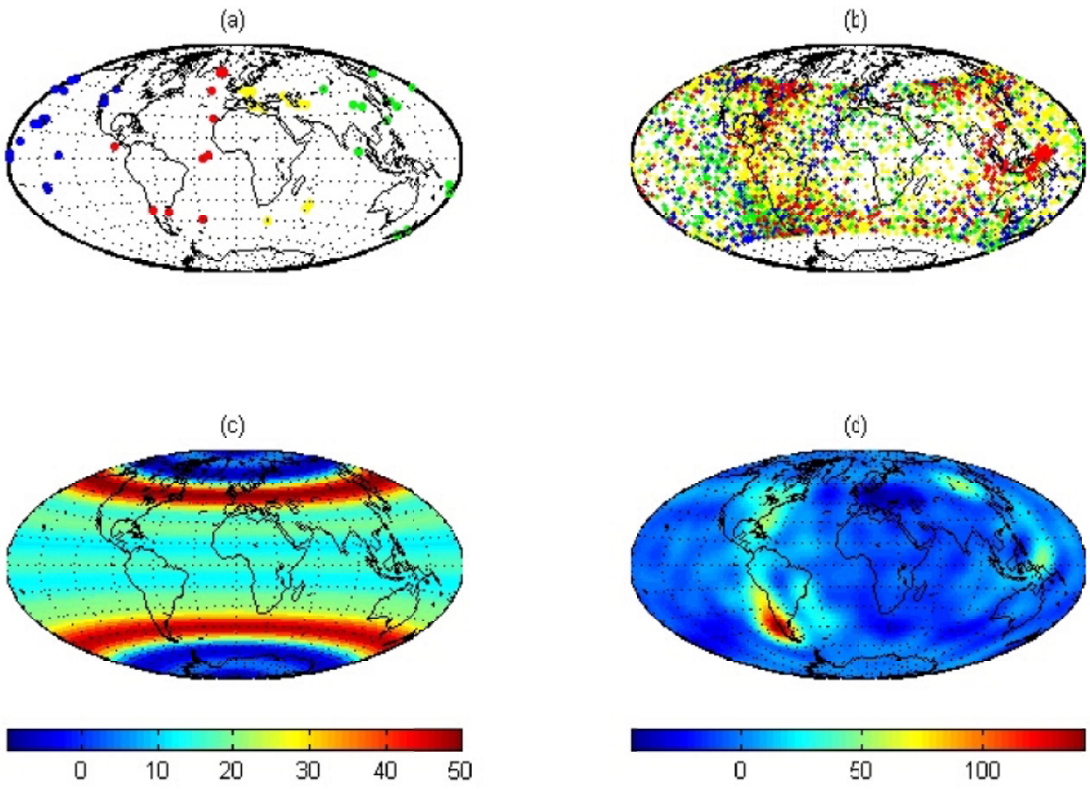

Fig. 2. Distribution of the sites and the transitional VGP ($Z^{(15)}(\hat{\mathbf{r}})$ and $W^{(15)}(\hat{\mathbf{r}})$): (a) The site distribution are divided into sectors, L_1 (yellow), L_2 (green), L_3 (blue) and L_4 (red) corresponding to 4 longitudinal sectors, (0, 90), (90,180), (−180, −90) and (−90, 0) respectively. (b) The distributions of the VGPs are plotted in yellow, green, blue, and red corresponding to the VGPs from the sites within the longitudinal sector L_1, L_2, L_3 and L_4 respectively (c) The zonal symmetric part of the VGP distribution in (b). (d) The non-zonal symmetric part of the VGP distribution in (b).

tion. In this paper, we first separate $D^{(L)}(\hat{\mathbf{r}})$ in terms of the zonal part $Z^{(L)}(\hat{\mathbf{r}})$—a sum of all zonal symmetries and the non-zonal part $W^{(L)}(\hat{\mathbf{r}})$—a sum of all non-zonal symmetries. We then separate $W^{(L)}(\hat{\mathbf{r}})$ in terms of the equatorial symmetries ${E_s}^{(L)}(\hat{\mathbf{r}})$—a sum of all terms in $W^{(L)}(\hat{\mathbf{r}})$ satisfying l-m=even number, and the equatorial asymmetries ${E_a}^{(L)}(\hat{\mathbf{r}})$—a sum of all terms in $W^{(L)}(\hat{\mathbf{r}})$ satisfying l-m=odd number, so,

$$\begin{aligned} D^{(L)}(\hat{\mathbf{r}}) &= Z^{(L)}(\hat{\mathbf{r}}) + W^{(L)}(\hat{\mathbf{r}}) \\ &= Z^{(L)}(\hat{\mathbf{r}}) + {E_s}^{(L)}(\hat{\mathbf{r}}) + {E_a}^{(L)}(\hat{\mathbf{r}}) . \end{aligned} \tag{8}$$

We shall illustrate the separations in the analyses of the VGP distribution in the following sections.

3. The Symmetries of the VGP Distribution during Polarity Reversal of the Earth's Magnetic Field

Two preferential VGP paths in the polarity reversal records along the American continents and East Asia-Australia were suggested over a decade ago (Clement, 1991; Laj *et al.*, 1991). Numerous studies on the VGP distribution have been carried out since then. While the statistical significance of the preferred VGP paths has been debated in some studies (Laj *et al.*, 1992a, b; Valet *et al.*, 1992; McFadden *et al.*, 1993), the effects on the VGP distribution due to various biases and noises in the paleomagnetic data are discussed in other studies (e.g. Langereis *et al.*, 1992; Weeks *et al.*, 1992; Prévot and Camps, 1993; Quidelleur and Valet, 1994; Coe and Liddicoat, 1994). These debates and discussions continue with almost every discovery of new reversal records (e.g. Channell and Lehman, 1997). The arguments on the two preferred paths originate from various statistical tests on the VGP distribution (in which the PDF of the VGP distribution is often implicit). The tests yielded competing and sometimes conflicting results (Laj *et al.*, 1992a, b; Valet *et al.*, 1992; McFadden *et al.*, 1993). While this is not an uncommon situation in statistical tests (because various assumptions are made in any statistical test), it is rather unfortunate that the methods are not themselves tested on the same set of points (e.g. an artificial set of points) so as to determine if these methods are suitable for the tasks and are self-consistent. In this paper, we illustrate some applications of the representation function in the analyses of the VGP distribution. The data set we use here is "Tran00" from the U.S. National Geophysical Data Center of NOAA. The ages of the records are all less than 10 million years and only transitional VGPs (within 55° of the equator) are used. The site and the VGP distribution are shown in Fig. 2(a) and 2(b). Our discussions consist of five parts, (1) the representation function for the VGP distribution in Fig. 2(b), (2) using the representation function to separate the zonal symmetries and the non-zonal symmetries in the VGP distribution, (3) evaluating biases in the non-zonal part of the VGP distribution, (4) estimating the persistent features in the non-zonal part of the VGP distribution and (5) a brief comparison between the methods we suggest here and the traditional methods used in

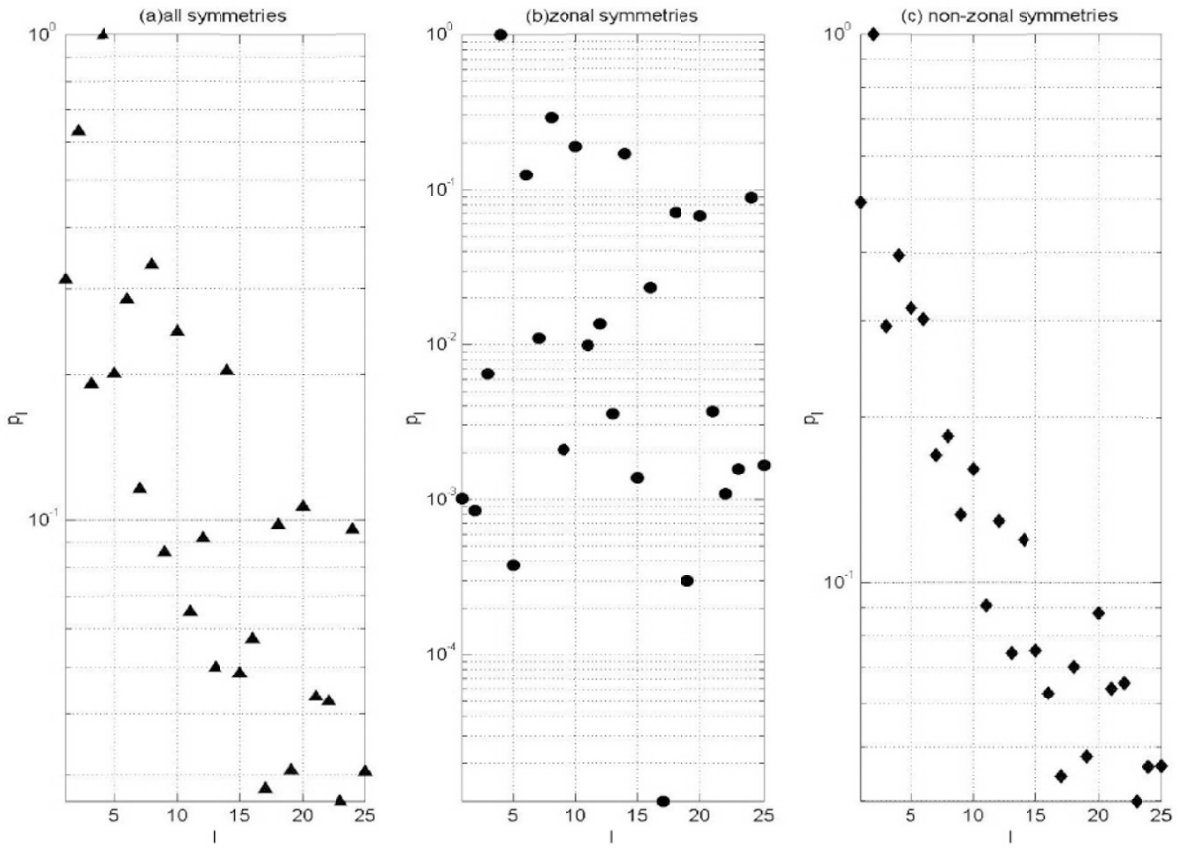

Fig. 3. The normalized power spectra for (a) the VGP distribution in Fig. 2(b), (b) the zonal symmetries in Fig. 2(c) and (c) the non-zonal symmetries in Fig. 2(d).

evaluating biases in the VGP distribution.

3.1 Representation function of the VGP distribution

Following (4), we obtain the coefficient d_l^m for the VGP distribution in Fig. 2(b) from,

$$d_l^m = \sum_{j=1}^{M} \sum_{i=1}^{N^j} \bar{Y}_l^m \left(\hat{\mathbf{p}}_i^j \right), \tag{9}$$

where $\hat{\mathbf{p}}_i^j$ is the ith VGP of the jth record in Fig. 2(b). The total number of the VGPs in the jth record is N^j, and the total number of records used is M. The set of the coefficients d_l^m obtained from (9) is unique. Using d_l^m, we can obtain the representation function $D\left(\hat{\mathbf{r}}\right)$ for VGP from (6). $D\left(\hat{\mathbf{r}}\right)$ exactly replicates the VGP distribution in Fig. 2(b) as such, $D\left(\hat{\mathbf{r}}\right) = 1$ at every $\hat{\mathbf{r}} = \hat{\mathbf{p}}_i^j$ and $D\left(\hat{\mathbf{r}}\right) = 0$ elsewhere. Of course, in the numerical computations, we can only obtain $D^{(L)}\left(\hat{\mathbf{r}}\right)$ from (5) instead of $D\left(\hat{\mathbf{r}}\right)$.

In all analyses given in this paper, we chose the truncation level of $D^{(L)}\left(\hat{\mathbf{r}}\right)$ at $L = 15$. This truncation level is obtained from the normalized power spectra $\mathbf{p}_l$ (defined in (7)) shown in Fig. 3(a) up to $l = 25$. Clearly, the primary signals in the power spectra are from p_l with $l < 15$. p_l for $l > 15$ tend to be flat and many of them are less than 10% of the maximum, implying randomness in the high order symmetries (with spatial wavelength less than 10 degrees) of the VGP distribution. Therefore, using $D^{(15)}\left(\hat{\mathbf{r}}\right)$ to represent primary information in the VGP distribution (Fig. 2(b)) seems adequate, if not very sufficient. Truncating at lower harmonic degrees such as $L = 15$ is also intuitively justified because of the low expectations on the quality of the reversal data set due to, e.g. grossly inadequate site coverage on the earth's surface and various experimental errors. Nonetheless, in order to be sure that the results we present in this paper are not greatly dependent on the truncation level, we actually carry out analyses at several truncation levels up to degree $L = 50$, and the results are consistent with those we present here. $D^{(15)}\left(\hat{\mathbf{r}}\right)$ is an image of the VGP distribution in Fig. 2(b) with spatial resolution of 10 degrees minimum half spatial wavelength. This roughly means that the figures (maps) in this paper are particularly sensitive to the signals in the VGP distribution that have a half spatial wavelength longer than 10 degrees.

3.2 Separation of the axial symmetries and the non-axial symmetries in the VGP distribution

The function $D^{(15)}\left(\hat{\mathbf{r}}\right)$ is separated into the zonal and the non-zonal symmetric parts, $Z^{(15)}\left(\hat{\mathbf{r}}\right)$ and $W^{(15)}\left(\hat{\mathbf{r}}\right)$ defined in (8). The maps for $Z^{(15)}\left(\hat{\mathbf{r}}\right)$ and $W^{(15)}\left(\hat{\mathbf{r}}\right)$ are shown in Fig. 2(c) and 2(d) respectively. The physical meanings of the scales in Fig. 2(c) and 2(d) are different from those in Fig. 1(b), 1(c) and 1(d). The values in Fig. 2(c) represent the geographic variations of the zonal part of the VGP distribution, and the values in Fig. 2(d) represent the geographic variations of the non-zonal part of the VGP distribution. However, the scale of the sum of the two maps has the same physical meanings as those of the Fig. 1(b), 1(c) and 1(d), it represents an image $D^{(15)}\left(\hat{\mathbf{r}}\right)$ of the VGP distribution

(Fig. 2(b)) "seen" at truncation level $L = 15$. As $L \to \infty$, $D^{(15)}\left(\hat{\mathbf{r}}\right) \to D\left(\hat{\mathbf{r}}\right)$ which replicates the VGP distribution in Fig. 2(b). Geometrically, the zonal part represents the patterns in the VGP distribution that are independent of the longitudes and the non-zonal part represents the longitudinally dependent patterns in the VGP distribution. Obviously, this type separation facilitates the detailed analysis of a particular class of the symmetries by isolating it from the original VGP distribution (without affecting the other symmetries whatsoever). The contributions to the VGP distribution (Fig. 2(b)) from the zonal and the non-zonal parts may be compared by using two normalized power spectra for $Z^{(15)}\left(\hat{\mathbf{r}}\right)$ (computed from (7) by using d_l^m with $m = 0$) and $W^{(15)}\left(\hat{\mathbf{r}}\right)$ (computed from (7) by using d_l^m with $m \neq 0$) shown in Fig. 3(b) and 3(c) respectively.

The large signals in the zonal part (Fig. 2(c)) are concentrated at the latitudes +/− 55 degrees and are obviously due to our selection of the VGP latitudes. However, this selection of the VGPs latitudes does not significantly affect the non-zonal symmetries in Fig. 2(d) because the longitudinal distribution of the VGPs at the latitudes higher than +/− 55 degrees is roughly uniform with strong axial symmetries and very weak non-zonal symmetries (we verified this). Nevertheless, because of the artificial restrictions of the VGP latitudes, all maps we present in this paper are valid only in the region between 55 and −55 degrees latitudes. The signals in the non-zonal part (Fig. 2(d)) are concentrated strongly along the longitudes of the east coast of the North American continent and relatively weakly along the longitudes of East Asia-Australia. In view of the fact that the zonal part (Fig. 2(c)) is unrelated to the paleomagnetic interests concerning the longitudinally dependent patterns in the VGP distribution, our analyses in this paper are only on the non-zonal part of the VGP distribution in Fig. 2(d).

3.3 Evaluation of biases in the VGP distribution

The patterns in the VGP distribution (Fig. 2(b)) and its non-zonal part (Fig. 2(d)) are contentious because of various biases in the paleomagnetic data set. For instance, in the present data set the maximum of the VGPs contributed by a reversal record is 274 and minimum is 3, with the mean and the standard deviation being 37 and 47 respectively. The number of the VGPs in a reversal record represents the number of the temporal samplings of the data at the site where the reversal record is recovered. A reversal record consisting of large number of the VGPs is called a long reversal record, and a reversal record consisting of small number of the VGPs is called a short reversal record. Apart from a few exceptions, the majority of long reversal records are sedimentary records, and the majority of short reversal records are lava records. The VGP distribution (Fig. 2(b)) consists of both long and short reversal records and therefore is always a biased VGP distribution. The effect of the biases is that the patterns in the VGP distribution may be greatly influenced by only long reversal records, and the contributions from short reversal records are relatively reduced. Here, we propose a method using the representation function to evaluate biases and to estimate the persistent patterns in the VGP distribution. We first outline the general procedures of the method. We then illustrate the method in specific examples.

3.3.1 The representation function of the weighted VGP distribution The notion of bias in a VGP distribution may be generally stated as: a group of VGPs makes far more contribution than other VGPs due entirely to some artificial factors. It follows that the evaluations of biases are to observe variations of the patterns in the VGP distribution as the contributions of these dominant VGPs are reduced (or equivalently, the contributions from the less dominant VGPs are increased). Obviously, these evaluations are possible only if the contribution of an individual VGP to the VGP distribution can be arbitrarily adjusted. In order to adjust the contribution of a VGP in Fig. 2(b), we modify d_l^m in (9) as,

$$\tilde{d}_l^m = \sum_{j=1}^{M} \sum_{i=1}^{N^j} k_i^j \bar{Y}_l^m \left(\hat{\mathbf{p}}_i^j\right), \tag{10}$$

where, $k_i^j \geq 0$ represents the significance of a point $\hat{\mathbf{p}}_i^j$. Two specific cases are $k_i^j = 1$ and $k_i^j = 0$, corresponding to the original and the removal of a VGP, $\hat{\mathbf{p}}_i^j$ respectively. Using $\tilde{d}_l^m$, the corresponding representation function of the weighted VGP distribution denoted as $\tilde{D}\left(\hat{\mathbf{r}}\right)$ can then be obtained from (6). $\tilde{D}\left(\hat{\mathbf{r}}\right)$ satisfies, $\tilde{D}\left(\hat{\mathbf{r}}\right) = k_i^j$ for every $\hat{\mathbf{r}} = \hat{\mathbf{p}}_i^j$, and $\tilde{D}\left(\hat{\mathbf{r}}\right) = 0$ elsewhere. The function $\tilde{D}\left(\hat{\mathbf{r}}\right)$ represents a set of the VGPs having the same geographic locations as those in Fig. 2(b), but a number k_i^j is now attached to each VGP indicating its significance. The biases in the VGP distribution can then be evaluated in the following steps:

(A) We first define a relationship $k_i^j = F_i^j[\alpha]$ to adjust the significance of a VGP, $\hat{\mathbf{p}}_i^j$ such that k_i^j of a VGP which makes a dominant contribution in the original VGP distribution (e.g. the VGPs from long reversal records) is gradually reduced and k_i^j of a VGP which makes little contribution in the original VGP distribution (e.g. the VGPs from short reversal records) is gradually increased in progressive steps marked by increasing value of α.

(B) At each step (at each α), a set of $\tilde{d}_l^m$ (a "new VGP distribution") is obtained from (10). We denote the "new VGP distribution" as $\tilde{D}_\alpha^{(L)}(.)$ for the step α (obtained from (5)). Following (8), denote $\tilde{W}_\alpha^{(L)}(.)$, $\tilde{E}_{s\alpha}^{(L)}(.)$ and $\tilde{E}_{a\alpha}^{(L)}(.)$ as the non-zonal part, the equatorially symmetric part and the equatorially asymmetric part (of the non-zonal part) of the "new VGP distribution" respectively. The "new VGP distribution" has the exactly the geographic distribution as the original VGP distribution, but the contribution of each VGP is changed.

(C) As k_i^j varies (as α increases), the biases in the VGP distribution vary and are reversed (e.g. the biases in the original VGP distribution due to the dominant contributions from long reversal records are gradually reversed to the biases due to the contributions from short reversal records.). The effects of biases in the original VGP distribution can now be evaluated by inspecting the variations in a series of maps, $\tilde{D}_\alpha^{(L)}(.)$, $\tilde{W}_\alpha^{(L)}(.)$, $\tilde{E}_{s\alpha}^{(L)}(.)$ and $\tilde{E}_{a\alpha}^{(L)}(.)$. The patterns that are not persistent and unstable in the maps are the artifacts due to biases in the original VGP distribution.

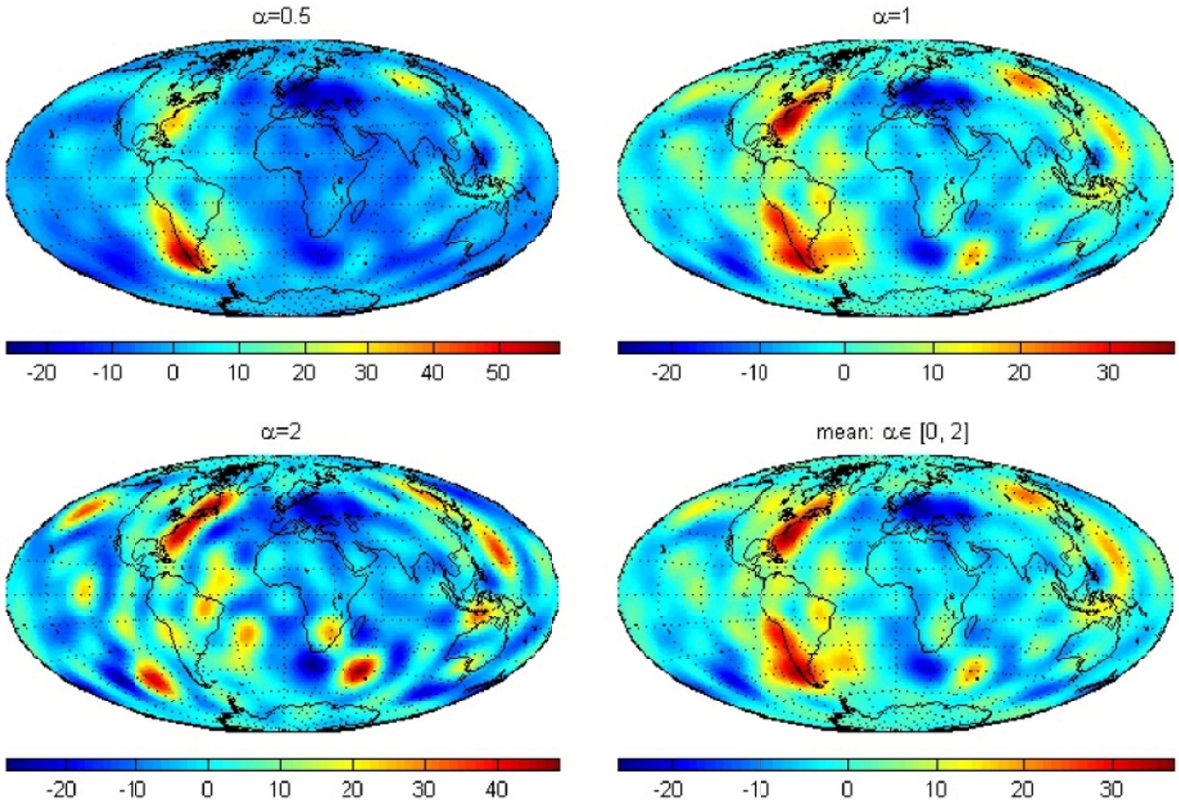

Fig. 4. The effects of biases due to uneven temporal samplings of the data $\tilde{W}_{\alpha}^{(15)}(\hat{\mathbf{r}})$ and the persistent patterns $\bar{W}^{(15)}(\hat{\mathbf{r}})$ in the non-zonal part of the VGP distribution.

(D) The patterns in the maps that persist throughout the evaluations (with relatively small variations in its geographic locations and amplitudes) are unlikely affected by biases. Obviously, it is not practical to display a series of maps in the paper. We find that the average functions, denoted as $\bar{W}^{(L)}(.)$, $\bar{E}_s^{(L)}(.)$ and $\bar{E}_a^{(L)}(.)$, for all maps of $\tilde{W}_{\alpha}^{(L)}(.)$, $\tilde{E}_{s\alpha}^{(L)}(.)$ and $\tilde{E}_{a\alpha}^{(L)}(.)$ adequately illustrated (at least in the examples given in this paper) the persistent patterns "seen" during the evaluations. However $\bar{W}^{(L)}(.)$, $\bar{E}_s^{(L)}(.)$ and $\bar{E}_a^{(L)}(.)$ are not the "optimal estimates" of the persistent patterns in the VGP distribution in any quantitative sense whatsoever.

3.3.2 Evaluating biases due to uneven temporal sampling of the data In this section, we evaluate biases in the VGP distribution (Fig. 2(b)) due to uneven temporal sampling of the data. Following step (A), we define k_i^j as,

$$k_i^j = \left(1/N^j\right)^{\alpha}, \quad \text{for} \quad \alpha \geq 0, \tag{11}$$

for the VGPs in jth reversal record. The relationship between significance of a VGP and the length of the corresponding reversal record in (11) is reciprocal. As α increases, the contributions from long reversal records are reduced more severely relative to those from short reversal records. For example, the significance of each VGP in a reversal record consisting of 100 VGPs is respectively reduced to 10% for $\alpha = 1$ and 1% for $\alpha = 2$ relative to a VGP in a reversal record consisting of 10 VGPs. For the VGPs in the same reversal record (or in the reversal records of same length), the significances are identical throughout the test. In the test, we use α ranging from 0 to 2 in a step of 0.1. Following step (B), we compute a set of $\tilde{d}_l^m$ up to $l = 25$ for each α ($\alpha = 0, 0.1, 0.2, 0.3, \ldots, 2$) by using (10) and (11). We obtain total 21 sets of $\tilde{d}_l^m$. We then compute $\tilde{W}_{\alpha}^{(15)}(\hat{\mathbf{r}})$ from each set of $\tilde{d}_l^m$ (we use $\tilde{d}_l^m$ with $m \neq 0$). Following step (C), we evaluate biases by inspecting a series of maps $\tilde{W}_{\alpha}^{(15)}(\hat{\mathbf{r}})$ shown in Fig. 4 for $\alpha = 0.5, 1, 2$. The values in each of these maps represent the geographic variations of the non-zonal symmetric part of VGP distribution (Fig. 2(b)) with each VGP being weighted according to (11). The maps themselves represent the changes in the non-zonal symmetric part of the original VGP distribution (Fig. 2(d)), as the contributions from long reversal records are gradually reduced relative to the contributions from short reversal records. The changes in Fig. 4 suggest that the non-zonal part (Fig. 2(d)) of VGP distribution (Fig. 2(b)) is affected by biases due to uneven temporal samplings of the data. Following step (D), the patterns, $\bar{W}^{(15)}(\hat{\mathbf{r}})$ in Fig. 4, that are persistently seen throughout the maps $\tilde{W}\alpha^{(15)}(\hat{\mathbf{r}})$ are along the longitudes of the east coast of the American continents and along the longitudes of East Asia. As we stated in (D), $\bar{W}^{(15)}(\hat{\mathbf{r}})$ is used only to qualitatively illustrate the persistent patterns and its relative geographic variations that we saw in a set of maps $\tilde{W}_{\alpha}^{(15)}(\hat{\mathbf{r}})$.

3.3.3 Evaluating the biases due to uneven temporal and spatial samplings of the data In this section, we modify the evaluation in Section 3.3.2 by taking into account of biases due to uneven geographic distribution of the sites

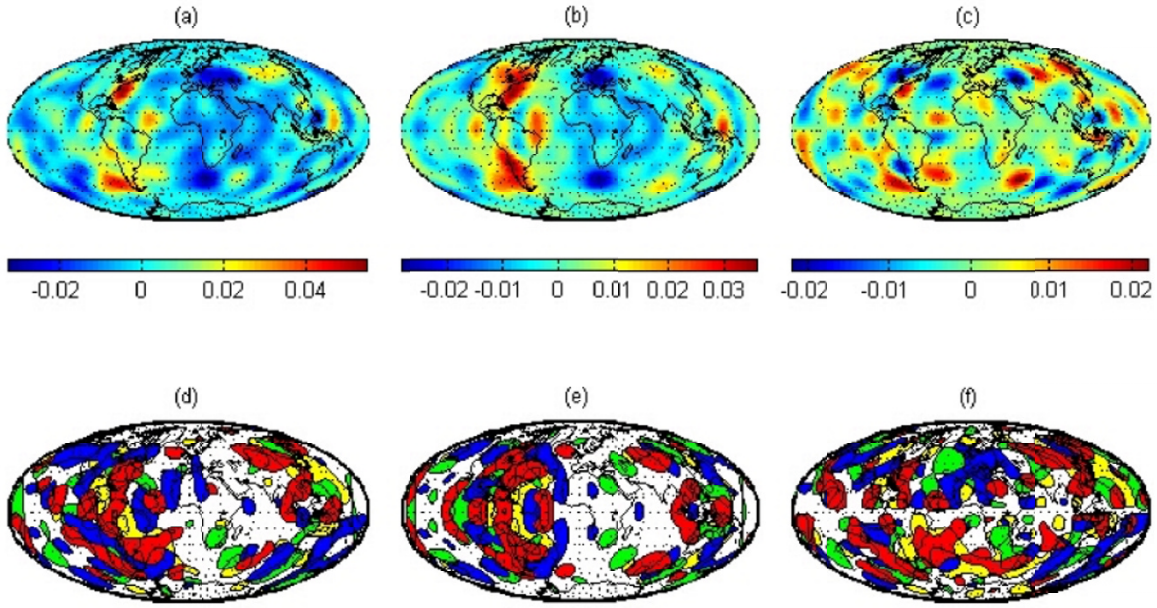

Fig. 5. The persistent patterns in the VGP distribution (a) $\bar{W}^{(15)}\left(\hat{\mathbf{r}}\right)$, (b) $\bar{E}_s^{(15)}\left(\hat{\mathbf{r}}\right)$, (c) $\bar{E}_a^{(15)}\left(\hat{\mathbf{r}}\right)$, (d) the patches of $\bar{W}^{(15)}\left([L_i]\right)$, (e) the patches of $\bar{E}_s^{(15)}\left([L_i]\right)$ and (f) the patches of $\bar{E}_a^{(15)}\left([L_i]\right)$.

(Fig. 2(a)). We first divide the site distribution in to four longitudinal sectors. The sites within each longitudinal sector and the VGPs contributed by the reversal records obtained at these sites are designated by the same colour as shown in Fig. 2(a) and 2(b) respectively. The total number of the VGPs contributed by the reversal records obtained within each longitudinal sector of the sites are $N_v\left(L_1\right) = 3092$, $N_v\left(L_2\right) = 878$, $N_v\left(L_3\right) = 520$ and $N_v\left(L_4\right) = 481$ respectively. The differences in $N_v\left(L_i\right)$ roughly reflect both the uneven spatial distribution of the sites and the uneven contributions to the VGP distribution from the reversal records obtained within different longitudinal sectors. Using the exactly same procedures (and the same range of $\alpha = 0, 0.1, 0.2, \ldots, 2$) discussed in Section 3.3.2, we first evaluate biases in a VGP distribution contributed by the reversal records obtained at the sites within each of the four longitudinal sectors (the VGPs are plotted by same colour in Fig. 2(b)) due to uneven temporal samplings of the data. For each VGP distribution, we obtain 21 sets of the coefficients $\tilde{d}_l^m$ and three sets of maps $\tilde{W}_\alpha^{(15)}\left(\hat{\mathbf{r}} \in L_i\right)$, $\tilde{E}_{s\alpha}^{(15)}\left(\hat{\mathbf{r}} \in L_i\right)$ and $\tilde{E}_{a\alpha}^{(15)}\left(\hat{\mathbf{r}} \in L_i\right)$ (21 maps in each set). For each α, we divide $\tilde{W}_\alpha^{(15)}\left(\hat{\mathbf{r}} \in L_i\right)$, $\tilde{E}_{s\alpha}^{(15)}\left(\hat{\mathbf{r}} \in L_i\right)$ and $\tilde{E}_{a\alpha}^{(15)}\left(\hat{\mathbf{r}} \in L_i\right)$ by the corresponding $N_v\left[L_i\right]$ and then summarize the functions to obtain $\tilde{W}_\alpha^{(15)}\left(\hat{\mathbf{r}}\right)$, $\tilde{E}_{s\alpha}^{(15)}\left(\hat{\mathbf{r}}\right)$ and $\tilde{E}_{a\alpha}^{(15)}\left(\hat{\mathbf{r}}\right)$ as,

$$\tilde{W}_\alpha^{(15)}\left(\hat{\mathbf{r}}\right) = \sum_{i=1}^{4} \left(N_v\left[L_i\right]\right)^{-1} \tilde{W}_\alpha^{(15)}\left(\hat{\mathbf{r}} \in L_i\right) \quad (12a)$$

$$\tilde{E}_{s\alpha}^{(15)}\left(\hat{\mathbf{r}}\right) = \sum_{i=1}^{4} \left(N_v\left[L_i\right]\right)^{-1} \tilde{E}_{s\alpha}^{(15)}\left(\hat{\mathbf{r}} \in L_i\right) \quad (12b)$$

$$\tilde{E}_{a\alpha}^{(15)}\left(\hat{\mathbf{r}}\right) = \sum_{i=1}^{4} \left(N_v\left[L_i\right]\right)^{-1} \tilde{E}_{a\alpha}^{(15)}\left(\hat{\mathbf{r}} \in L_i\right) \quad (12c)$$

Weighting $\tilde{W}_\alpha^{(15)}\left(\hat{\mathbf{r}} \in L_i\right)$, $\tilde{E}_{s\alpha}^{(15)}\left(\hat{\mathbf{r}} \in L_i\right)$ and $\tilde{E}_{a\alpha}^{(15)}\left(\hat{\mathbf{r}} \in L_i\right)$ by $\left(N_v\left[L_i\right]\right)^{-1}$ in (12(a), (b) and (c)) tend to reduce the relative contributions from the longitudinal sectors containing large number of the sites and contributing large number of the VGPs. Following step (C), by inspecting a series of maps $\tilde{W}_\alpha^{(15)}\left(\hat{\mathbf{r}}\right)$, $\tilde{E}_{s\alpha}^{(15)}\left(\hat{\mathbf{r}}\right)$ and $\tilde{E}_{a\alpha}^{(15)}\left(\hat{\mathbf{r}}\right)$ (which we do not show here), we observed that the variations in these maps are different from those in Fig. 4. This suggests that the non-zonal part (and its equatorially symmetric and asymmetric parts) of the VGP distribution are affected by biases not only due to uneven temporal samplings of the data (discussed in Section 3.3.3) but also due to uneven spatial distribution of the sites and the associated uneven contributions of the VGPs (the differences in $N_v\left[L_i\right]$). Following step (D), we illustrate the persistent patterns seen in the maps of $\tilde{W}_\alpha^{(15)}\left(\hat{\mathbf{r}}\right)$, $\tilde{E}_{s\alpha}^{(15)}\left(\hat{\mathbf{r}}\right)$ and $\tilde{E}_{a\alpha}^{(15)}\left(\hat{\mathbf{r}}\right)$, as $\bar{W}^{(15)}\left(\hat{\mathbf{r}}\right)$, $\bar{E}_s^{(15)}\left(\hat{\mathbf{r}}\right)$ and $\bar{E}_a^{(15)}\left(\hat{\mathbf{r}}\right)$ in Fig. 5(a), 5(b) and 5(c) respectively.

3.4 The persistent features in the VGP distribution

One of the purposes of evaluating biases in the VGP distribution is to qualitatively estimate the persistent patterns in the VGP distribution such as those shown in Fig. 5(a), 5(b) and 5(c), because these patterns likely constitute physical signals of the earth's magnetic field. In order to illustrate the persistent patterns in the VGP distribution contributed by the reversal records obtained within each of 4 longitudinal sectors respectively, we obtain persistent patterns $\bar{W}^{(15)}\left(\hat{\mathbf{r}} \in L_i\right)$, $\bar{E}_s^{(15)}\left(\hat{\mathbf{r}} \in L_i\right)$ and $\bar{E}_a^{(15)}\left(\hat{\mathbf{r}} \in L_i\right)$ from the maps $\tilde{W}_\alpha^{(15)}\left(\hat{\mathbf{r}} \in L_i\right)$, $\tilde{E}_{s\alpha}^{(15)}\left(\hat{\mathbf{r}} \in L_i\right)$ and $\tilde{E}_{a\alpha}^{(15)}\left(\hat{\mathbf{r}} \in L_i\right)$ for each L_i obtained in Section 3.3.3. We then plot the patches of $\bar{W}^{(15)}\left(\hat{\mathbf{r}} \in L_i\right)$, $\bar{E}_s^{(15)}\left(\hat{\mathbf{r}} \in L_i\right)$ and $\bar{E}_a^{(15)}\left(\hat{\mathbf{r}} \in L_i\right)$ in Fig. 5(d), 5(e) and 5(f) for each L_i. The colours of the patches correspond to those used in Fig. 2(a) for the sites. The patches show only positive parts (the accretions of the VGPs) of $\bar{W}^{(15)}\left(\hat{\mathbf{r}} \in L_i\right)$, $\bar{E}_s^{(15)}\left(\hat{\mathbf{r}} \in L_i\right)$ and $\bar{E}_a^{(15)}\left(\hat{\mathbf{r}} \in L_i\right)$ with magnitudes no less than 10% of the maximums in $\bar{W}^{(15)}\left(\hat{\mathbf{r}} \in L_i\right)$, $\bar{E}_s^{(15)}\left(\hat{\mathbf{r}} \in L_i\right)$ and $\bar{E}_a^{(15)}\left(\hat{\mathbf{r}} \in L_i\right)$ respectively.

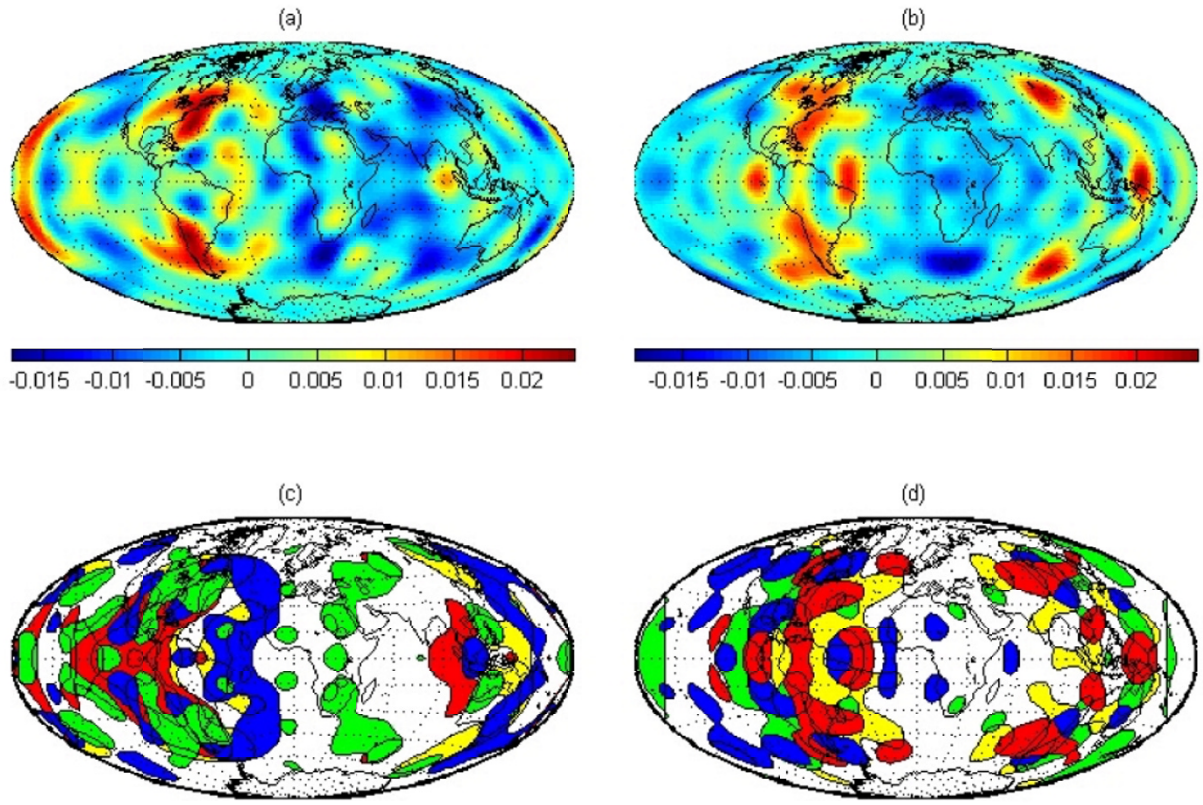

Fig. 6. The persistent patterns in the VGP distribution (a) normal to reverse polarity, $\bar{E}_s^{(15)}(\hat{\mathbf{r}})$, (b) reverse to normal polarity, $\bar{E}_s^{(15)}(\hat{\mathbf{r}})$, (c) the patches of $\bar{E}_s^{(15)}([L_i])$ for normal to reverse polarity and (d) the patches of $\bar{E}_s^{(15)}([L_i])$ for reverse to normal polarity.

We also evaluated biases in the VGP distributions for the reversals from normal to reversed (N-R) polarity and from reversed to normal (R-N) polarity due to uneven spatial and temporal samplings of the data by using the same method described in Section 3.3.3, and obtained the persistent patterns in the VGP distributions for two opposite reversals. For simplicity, we only illustrate the persistent patterns in $\bar{E}_s^{(15)}(\hat{\mathbf{r}})$ for N-R and for R-N in Fig. 6(a) and Fig. 6(b) respectively. The patches of $\bar{E}_s^{(15)}(\hat{\mathbf{r}} \in L_i)$ are shown in Fig. 6(c) and 6(d) respectively.

We find that the signals of large-scale concentrations persist in the equatorially symmetric part (of the non-zonal part) of the VGP distributions (Fig. 5(b), Fig. 6(a) and Fig. 6(b)). The strong signals broadly concentrate within two longitudinal confinements: one along the longitudes of the east coast of the North American continent and another (signals are relatively weak and vague) along the longitudes of East Asia-Australia. The patches (Fig. 5(e), Fig. 6(c) and Fig. 6(d)) show the broadly similar longitudinal confinements (but there are discrepancies between N-R and R-N reversals shown in Fig. 6(c) and Fig. 6(d) respectively). This suggests that the two longitudinal confinements in the VGP distributions are likely the global signals of the earth's magnetic field during the polarity reversals. The patches in Fig. 5(e), Fig. 6(c) and 6(d) also show preferential extensions in the Pacific Ocean, but the signals in the area of preferential extensions are weaker than those in the area of the longitudinal confinements. Whether or not these patterns are the true signals is an interesting point to be tested by future paleomagnetic data. We also found that there are no large-scale systematic patterns in the equatorial asymmetries of the non-zonal part of the VGP distribution (Fig. 5(c), we do not show maps of the equatorial asymmetries for N-R and R-N reversals, the situations are similar to those in Fig. 5(c)). This may suggest that the equatorial asymmetries in the VGP distributions are not well defined by the present data set. Whether or not there are systematic patterns in the equatorially asymmetric part of the VGP distribution should be reassessed as more data become available.

3.5 Discussion on the methods of evaluating biases in the VGP distribution

The data set of the reversal records contains other types of biases associated with the properties (e.g. the sedimentation rate) of the paleomagnetic recorders. The methods of evaluating biases in the VGP distribution we discussed in this paper take the advantage offered by the representation function that every point in the point distribution may be arbitrarily weighted. This facilitates the evaluation of any biases associated with the VGP distribution by modifying the impact of a VGP. The methods described in Section 3.3 are in many ways more flexible than the traditional methods. For instance, the biases in the VGP distribution are traditionally evaluated by first removing the "problematic" reversal records from the original data set to obtain a smaller subset of the data. The VGP distribution of the subset is then evaluated to determine whether or not the patterns in the original data set also persist in the patterns of the subset. If the patterns persist, then the patterns are robust, if the patterns do

not persist, then the patterns may be artifacts. The removal of the "problematic" reversal records would of course remove biases, but at the same time it would also reduce the site coverage on the earth's surface (unless of course the deleted data are nothing but noise). Therefore, if the number of the reversal records in the subset is far fewer than that in the original data set, then the selected subset of the data set is in fact more biased due to the inadequate and perhaps more biased distribution of the sites. Furthermore, reducing the original data set to a small subset would probably enhance other biases in the subset. The removal of any data is not required in the method we discussed, but is also accommodated as an extreme case by setting the significance of a VGP to zero.

Defining the weighting factor k_i^j in (11) is however not unique (the weighting factors may be defined by other reciprocal relationships). This non-uniqueness is because of the fact that we can only qualitatively define biases in the VGP distribution. If we can quantitatively define and evaluate biases (of any type), it would logically mean that we could extract an "idea" or estimate an "optimal" VGP distribution (with the associated error estimates) from a biased VGP distribution. We did not see how such undertakings for the paleomagnetic data set are logically possible. Nonetheless, in so long as k_i^j is defined following the basic requirement that biases in the original VGP distribution are progressively reduced (e.g. the weights of long reversal records are progressively reduced relative to short reversal records), we think that, logically, the outcome of these evaluations should be at least qualitatively consistent.

4. Conclusion

The primary objective in this paper is to introduce a representation function $D(\hat{\mathbf{r}})$ in (6) that uniquely, completely and quantitatively represents a geometrical object—a point distribution on the unit sphere. This representation function facilitates both evaluation and manipulation of a complex point distribution analytically. There is a wealth of theorems, formulas and operators associated with spherical harmonics, and by examining spherical point distributions in terms of the infinite series of spherical harmonics, this extensive machinery can be used to analyze spherical point sets. Two elementary applications of the representation function that we illustrate in this paper, via the analyses of the VGP distribution, are (a) separating various symmetries and (b) evaluating biases in the VGP distribution.

We find that there are two persistent longitudinal confinements in the equatorial symmetries of the non-zonal part of the transitional VGP distribution of the polarity reversals for the past 10 million years which are similar to the two preferred VGP paths suggested by other studies (Clement, 1991; Laj *et al.*, 1991). We also find that this equatorially symmetric part appears to have preferential extensions in the Pacific Ocean. This implies a difference between the geometric configurations of the earth's magnetic field in the Pacific hemisphere and those in the hemisphere of the Prime meridian during polarity reversal. However, the signals in the areas of the extensions are weak and need to be tested by new data.

Of course, in order to systematically analyze the physical signals in the VGP distribution more relevant to the causes of paleomagntism, a better data set and a more sophisticated analytic framework is needed to deal with the issues that we have not addressed. The advanced analytic framework should include more advanced applications of the representation function, the existing statistical methods and more input from our physical understanding of the earth's magnetic field. We think that the representation function of a point distribution discussed in this paper is essential to the development of such a framework.

Acknowledgments. Ji-Cheng Shao wish to acknowledge a JSPS Post-doctoral fellowship from the government of Japan. We also wish to thank the editor Dr. H. Tanaka, Dr. S. Bogue and an anonymous reviewer for their careful reviews on the manuscript and their constructive comments.

References

Backus, G., R. Parker, and C. Constable, *Foundation of Geomagnetism,* Cambridge University Press, Cambridge, 158 pp., 1996.

Channell, J. E. T. and B. Lehman, The last two geomagnetic polarity reversals recorded in high-deposition-rate sediment drifts, *Nature,* **389**, 712–715, 1997.

Clement, B. M., Geographical distribution of transitional VGPs: Evidence for non-zonal equatorial symmetry during the Matuyama-Brunhes geomagnetic reversal, *Earth planet. Sci. Lett.,* **104**, 48–58, 1991.

Coe, R. S. and J. C. Liddicoat, Overprinting of natural magnetic remanence in lake sediments by a subsequent high-intensity field, *Nature,* **367**, 57–59, 1994.

Fisher, N. I., T. Lewis, and B. J. J. Embleton, *Statistical Analysis of Spherical Data,* Cambridge University Press, Cambridge, 329 pp., 1987.

Laj, C., A. Mazaud, R. Weeks, M. Fuller, and E. Herrero-Bervera, Geomagnetic reversal paths, *Nature,* **351**, 447, 1991.

Laj, C., A. Mazaud, R. Weeks, M. Fuller, and E. Herrero-Bervera, Geomagnetic reversal paths, *Nature,* **359**, 111–112, 1992a.

Laj, C., A. Mazaud, R. Weeks, M. Fuller, and E. Herrero-Bervera, Statistical assessment of the preferred longitudinal bands for recent geomagnetic reversal records, *Geophys. Res. Lett.*, **19**, 2003–2006, 1992b.

Langereis, C. G., A. A. M. van Hoof, and P. Rochette, Longitudinal confinement of geomagnetic reversal paths as a possible sedimentary artefact, *Nature,* **358**, 226–230, 1992.

McFadden, P. L., C. E. Barton, and R. T. Merrill, Do virtual geomagnetic poles follow preferred paths during geomagnetic reversals?, *Nature,* **361**, 342–344, 1993.

Prévot, M. and P. Camps, Absence of preferred longitude sectors for poles from volcanic records of geomagnetic reversals, *Nature,* **366**, 53–57, 1993.

Quidelleur, X. and J.-P. Valet, Paleomagnetic records of excursions and reversals: Possible biases caused by magnetization artefacts, *Phys. Earth planet. Inter.*, **82**, 27–48, 1994.

Valet, J.-P., P. Tucholka, V. Courtillot, and L. Meynadier, Palaeomagnetic constraints on the geometry of the geomagnetic field during reversals, *Nature,* **356**, 400–407, 1992.

Weeks, R., M. Fuller, C. Laj, A. Mazaud, and E. Herrero-Bervera, Sedimentary records of reversal transitions—magnetization smoothing artefact or geomagnetic field behaviour?, *Geophys. Res. Lett.*, **19**, 2007–2010, 1992.

J.-C. Shao, Y. Hamano (e-mail: hamano@eps.s.u-tokyo.ac.jp), M. Bevis, and M. Fuller